This is the author's version of an article that has been published in this journal. Changes were made to this version by the publisher prior to publication.
The final version of record is available at http://dx.doi.org/10.1109/TIA.2017.2743200

A Comparative Study of Methods for Estimating Virtual Flux at the Point of Common Coupling in Grid Connected Voltage Source Converters with LCL Filter

Nurul Fazlin Roslan[♠♦], Jon Are Suul[♣], *Member, IEEE*, Joan Rocabert[♠], *Member, IEEE*, Pedro Rodriguez[♠], *Fellow, IEEE*

[♠] Technical University of Catalonia,
Research Center on Renewable Electrical Energy Systems (SEER Center),Terrassa, Spain
[♦] Universiti Kuala Lumpur, British Malaysian Institute, Gombak, Malaysia
[♣] SINTEF Energy Research, Trondheim, Norway

Abstract- Grid synchronization based on Virtual Flux (VF) estimation allows for control of grid-connected power converter without depending on AC-voltage measurements. This is useful in voltage-sensor-less applications for reducing cost and complexity of the control hardware, and can be utilized in case of limited reliability or availability of voltage measurements at the intended point of synchronization to the grid. However, for Voltage Source Converters (VSC) with LCL filters, the influence of the capacitor current must be taken into account to ensure accurate VF estimation at the Point of Common Coupling (PCC) with the grid. This paper presents a comparative evaluation of three VF-based methods for grid synchronization of VSCs with LCL filters, with three different ways of obtaining the capacitor current. The VF estimation in the first method is based only on the measured converter currents. The second method includes capacitor voltage measurements used for estimating the capacitor currents, while the capacitor currents are measured in the third approach. Comparative results from time-domain simulations are presented, demonstrating good performance of the estimation and accurate control of the active and reactive power at the PCC with all three methods, as long as sufficiently accurate filter parameters and current measurements are available. However, the approach based on capacitor current measurements is sensitive to noise due to the high ripple current compared to the fundamental frequency current in the capacitors. The operation of a converter with VF-based grid synchronization including estimation of the capacitor current is demonstrated by experimental results, verifying the voltage sensor-less operation with LCL-filter.

Keywords- Voltage Source Converter, Virtual Flux Estimation, Proportional Resonant Current Controller, LCL-Filter.

Copyright (c) 2017 IEEE. Personal use is permitted. For any other purposes, permission must be obtained from the IEEE by emailing pubs-permissions@ieee.org.

This is the author's version of an article that has been published in this journal. Changes were made to this version by the publisher prior to publication.
The final version of record is available at http://dx.doi.org/10.1109/TIA.2017.2743200

1. Introduction

Power electronic converter technology enables flexible interconnection between renewable energy generation systems and the electrical network. Therefore, power converters and their control systems play an important role in the grid integration of Renewable Energy Systems (RES) like wind turbines and photovoltaic installations [1]. In most of the RES based generation systems two-level VSCs in the low voltage range are used as the power conversion stage, due to good trade-offs between cost-performance and controllability [2]-[4]. However, VSC topologies are also suitable for medium voltage applications, and are becoming widely used in high voltage direct current (VSC-HVDC) applications [5]-[7].

In grid-connected applications of VSCs, control of the active and reactive power exchanged with the network is high importance. Thus, accurate synchronization to the voltage at the point where the power flow should be controlled is crucial. Indeed, several methods for grid synchronization based on voltage measurements have been proposed [8]-[12]. Voltage sensor-less control is an alternative approach for grid synchronization, based on estimation of the grid voltage conditions without depending on ac-voltage sensors [13]-[17]. By applying Virtual Flux (VF) estimation, it is possible to achieve a simple approach for grid synchronization and control of power converters, based only on the measured converter currents and the dc voltage of the converter. This feature can be utilized to reduce the number of sensors, but it also makes it possible to estimate the voltage at remote points that are not easily available for measurements [18]-[19]. However, implementation of a control system based on VF estimation depends on access to accurate parameters for the filter interfacing the converter to the ac grid.

Grid synchronization based on VF estimation can be combined with different types of control strategies, including Direct Power Control (DPC) [20]-[22] or Voltage Oriented Control (VOC) [23]. Indeed, early studies of VF estimation were based on direct power control (VF-DPC), where it was demonstrated that similar performance could be achieved as for original DPC method [24]-[25]. In [26], the operation of VF based control, considering a VF oriented control (VFOC) and a VF-DPC implementation, have been compared with the voltage based control (VOC and V-DPC). An improved VF-based synchronization strategy including estimation of the filter inductance and combined with a predictive DPC control algorithm (VF-P-DPC) was presented in [27]. However, these studies considered mainly synchronization of VSCs to balanced grids, under the assumption of connection to the grid by L- or LC-filters. In [28], a method for sensor-less operation based on a Positive and Negative Sequence (PNS) VF model was presented, where the VF estimation was obtained by using two cascaded Low-Pass (LP) filters. The cut-off frequency of the LP filters was identical to the frequency of the grid, in order to obtain a 90° phase shift for fundamental frequency components, which was utilized in the VF estimation. The same filtering approach was also used for the in-quadrature signal generation needed for Positive and Negative Sequence (PNS) separation. Since LP-filters were used, a drift

Copyright (c) 2017 IEEE. Personal use is permitted. For any other purposes, permission must be obtained from the IEEE by emailing pubs-permissions@ieee.org.

This is the author's version of an article that has been published in this journal. Changes were made to this version by the publisher prior to publication.
The final version of record is available at http://dx.doi.org/10.1109/TIA.2017.2743200

compensation technique was included in the practical implementation, in order to achieve an offset-free VF estimation and to avoid degradation of estimation accuracy during grid frequency variations. However, [28] was based on cascaded VF estimation and PNS separation, resulting in a relatively slow transient response. Thus, the works presented in [29]-[31] attempted to improve the dynamic performance by utilizing a set of Dual Second-Order Generalized Integrators for VF-estimation (DSOGI-VF) with inherent sequence separation. The DSOGI-VF estimation also allows for inherent frequency adaptive operation.

The mentioned examples of VF-based grid synchronization have considered mainly power converters connected to the grid through L- or LC filters. However, in case of LCL-filters, it can be necessary to control the power flow on the grid-side of the second filter inductor. Thus, for VF-based synchronization to the grid-side of an LCL-filter, it is necessary to consider the influence of the currents in the filter capacitors. Only a few studies have previously considered VF-based voltage-sensor-less grid synchronization with LCL-filters [3], [32]-[35]. The DSOGI-VF estimation described in [36] is an extended version of the work presented in [29]-[31] taking into account the VSC connected to the grid through the LCL filter and PR current controller is used as an inner control of the VSC. However, as discussed in [3], [19] VF estimation can also be useful if capacitor voltage measurements are available.

In this paper, three options for VF-based synchronization to the PCC is studied for converters with LCL filters, and PNS separation is taken into account as part of the VF estimation. Estimation of the grid-side current is also included in the VF-based synchronization strategy, in order to obtain an accurate voltage or flux across the grid-side inductor. This kind of estimation strategy has not been studied in detail in the existing literature, and it is the main contribution of this work. Thus, three different approaches for VF estimation at the PCC will be presented and compared. Indeed, the objective of the synchronization strategy is to ensure accurate control of the active and reactive power injected to the PCC. Since the VF-estimation is implemented in the stationary reference frame, Proportional Resonant (PR) current controllers will be used as the inner loop control of the VSC. For extending the work from [37], further simulations of the studied VF estimation methods and experimental verification of VF-based voltage sensor-less operation of a three phase VSC will be presented in this paper. As it will be shown in both simulation and experiments, the VF estimation is reliable in estimating the conditions of the grid-side voltage conditions, and can provide the basis for control of the active and reactive power injection without voltage sensors at the PCC and/or currents sensors in the grid-side inductance of the LCL-filter.

The paper continues with an overview of the proposed VF estimation for VSCs with LCL filter, including a brief introduction of the PR current controller used in the inner control loop of the VSC as well as the current reference generation. Then, the three investigated methods for VF estimation with LCL filters are presented in section 3. Furthermore, the simulation cases are

Copyright (c) 2017 IEEE. Personal use is permitted. For any other purposes, permission must be obtained from the IEEE by emailing pubs-permissions@ieee.org.

This is the author's version of an article that has been published in this journal. Changes were made to this version by the publisher prior to publication.
The final version of record is available at http://dx.doi.org/10.1109/TIA.2017.2743200

presented and the obtained results are compared and discussed in section 4, before experimental verification of voltage-sensor-less VF-based control is presented in section 5.

2. System configuration and VF-based control for VSC with LCL Filter

The study case that will be considered in this paper is shown in Fig. 1, including a VSC connected to the grid through an LCL filter. In this configuration, VF estimation is utilized for synchronizing the converter control system to the voltage conditions at the PCC. Thus, the resistive and inductive voltage or flux across the second inductor, L_2, and the equivalent impedance Z_T of the transformer must be taken into account in the VF estimation.

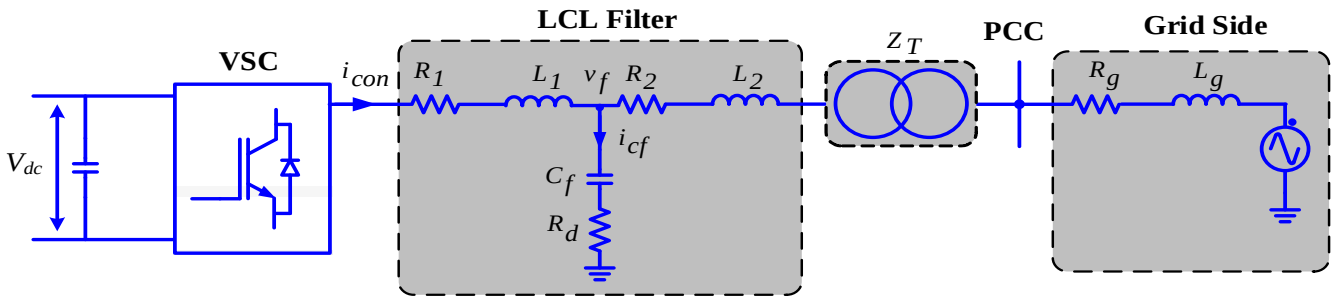

Fig. 1. An overview of the structure of investigated system.

The VF estimation permits to estimate the grid voltage condition as long as the filter parameters are available. This can be considered feasible, since the filter should be designed as a part of the converter configuration. It should be noted that the VF estimation is based on the current measurement at the convertor side, i_{con}, while the converter output voltage used for the VF estimation is calculated from the internal reference signals in the control system and the measured dc voltage.

Considering the structure shown in Fig. 1 and assuming that the capacitor current, i_{cf}, cannot be ignored, three possible methods are investigated for including the capacitor current in the VF estimation. The first method is based on performing an estimation without additional sensors in the LCL-filter. Thus, the capacitor current will be estimated from the virtual flux at the filter capacitor. The second possible method for obtaining the capacitor current is based on using a voltage sensor to measure the capacitor voltage, v_f, which can be used for estimating the capacitor current. Finally, the third method implements the VF-estimation by means of using a direct measurement of the capacitor current. However, a brief introduction to VF estimation and the assumed control system is presented before discussing the particular implementations of the three investigated methods for VF estimation in detail.

Copyright (c) 2017 IEEE. Personal use is permitted. For any other purposes, permission must be obtained from the IEEE by emailing pubs-permissions@ieee.org.

This is the author's version of an article that has been published in this journal. Changes were made to this version by the publisher prior to publication.
The final version of record is available at http://dx.doi.org/10.1109/TIA.2017.2743200

2.1 Introduction to VF estimation

Considering that the control implementation in this work is carried out in a stationary reference frame, the ideal estimation of virtual flux can be described according to (1).

$$\Psi_{\alpha\beta}(t) = \int V_{conv} dt + \Psi_0 = \int m_{ref,\alpha\beta} \left(\frac{V_{dc}}{2} \right) dt + \Psi_0 \quad (1)$$

The basis for the estimation is that the converter output voltage, V_{conv} is obtained by multiplying the dc-link voltage with the reference signal for the Pulse-Width Modulation (PWM) of the converter output voltage. However, the voltage drop caused by the conduction losses of the converter and the primary filter inductor, represented by the equivalent resistance R_1, should be taken into account in the converter output voltage before the integration in (1).

The VF estimation methods considered in this paper are designed to be suitable for both balanced and unbalanced conditions. Furthermore, the ideal integration in (1) can be sensitive to drift and offset in the VF estimation. Thus, the VF estimation used in this work is based on the Dual Second Order Generalized Integrator with Quadrature Signal Generator (DSOGI-QSG) and a Frequency Locked Loop (FLL), as proposed in [30]-[31] and [36] - [37].

2.2 Frequency Adaptive of DSOGI-FLL

In this paper the DSOGI-FLL is used for synchronization purposes, whose main operation principle and dynamic performance is presented in [38]. As it is described in the aforementioned paper, the frequency input needed by the DSOGI-QSG, used in this work, is available from the FLL output. By using the FLL, the center frequency of the SOGI resonators, and by that the overall DSOGI-QSG structure, will be automatically adapted to variations in the grid frequency. Since the SOGIs are working at the same frequencies, only one FLL will be used in this work. The input of the SOGI is the signal to be integrated, namely v. If the input signal is sinusoidal, both the direct output voltage v' and the in-quadrature signal qv' will always be sinusoidal. The two outputs from the SOGI-QSG will always have the same amplitude if the input signal and the resonance frequency of the SOGI are equal.

In AC systems the frequency is a global magnitude. In this work, the FLL is responsible to make the synchronization process adaptive to the frequency changes. Nevertheless, the grid frequency is usually close to the nominal value and does not experience sudden changes. Therefore a nominal frequency feedforward, ω_{ff}, is used in order to enhance the dynamical performance of the FLL initialization. This feedforward signal is an offset which allows the integrator of the FLL to track only the deviations from the nominal grid frequency, but the DSOGI-FLL is self-adaptive and would always track the final frequency whatever it will be.

Copyright (c) 2017 IEEE. Personal use is permitted. For any other purposes, permission must be obtained from the IEEE by emailing pubs-permissions@ieee.org.

This is the author's version of an article that has been published in this journal. Changes were made to this version by the publisher prior to publication.
The final version of record is available at http://dx.doi.org/10.1109/TIA.2017.2743200

In the DSOGI the direct output voltage *v'* will be in phase with the input voltage *v*, while *qv'* will lag the direct output voltage *v'* by 90°. The error between the input and direct output voltage is denoted as '*e'* and the frequency of the system is symbolized as ω'. The in-quadrature signal *qv'* from the SOGI-QSGs provides the 90° shifted signals needed for VF estimation, and combined with the direct output signal *v'*, the orthogonal signals required for sequence separation will be inherently available in a DSOGI-VF estimation.

Fig. 2 (a) shows the diagram of a single block of a Second Order Generalized Integrator configured as a Quadrature Signal Generator (SOGI-QSG). Fig. 2 (b) on the other hands shows the structure of the FLL with a normalized gain and the simplified diagram of the FLL is shown in Fig. 2 (c). The input of the FLL is provided by the SOGI-QSG as it can be seen in Fig. 2 where the error signal and the in-quadrature output signal both in alpha beta components have been used.

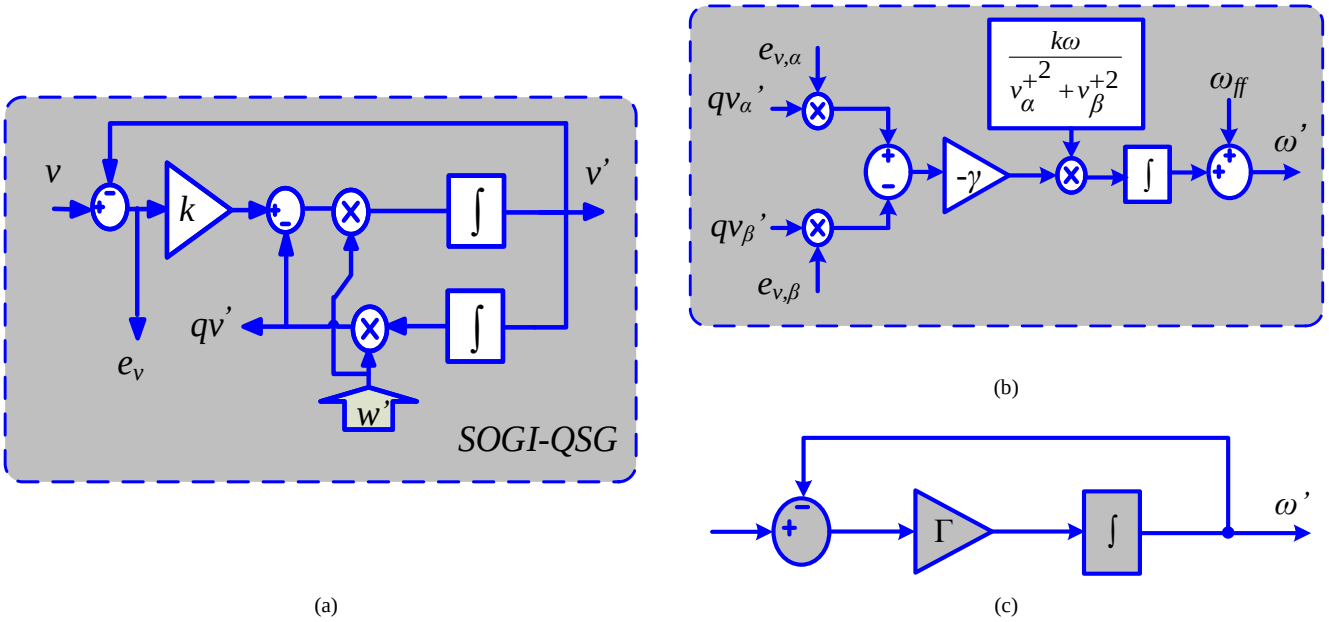

Fig. 2. SOGI-FLL block diagram. (a) Second Order Generalized Integrator with Quadrature Signal Generator (b) Frequency Locked Loop with Gain Normalization and (c) Simplified Frequency Adaption System of FLL.

The transfer functions of the SOGI-QSG for the direct output voltage, *v'* and the in-quadrature output voltage, *qv'* with respect to the input voltage, *v* are given by (2) and (3) respectively [1].

$$D(s) = \frac{v'}{v}(s) = \frac{k\omega' s}{s^2 + k\omega' s + \omega'^2} \tag{2}$$

$$Q(s) = \frac{qv'}{v}(s) = \frac{k\omega'^2}{s^2 + k\omega' s + \omega'^2} \tag{3}$$

Copyright (c) 2017 IEEE. Personal use is permitted. For any other purposes, permission must be obtained from the IEEE by emailing pubs-permissions@ieee.org.

This is the author's version of an article that has been published in this journal. Changes were made to this version by the publisher prior to publication.
The final version of record is available at http://dx.doi.org/10.1109/TIA.2017.2743200

In order to understand how the system adapt to the frequency changes, it is worth to consider the behavior of the FLL by looking at the relationship between the error signal, ε_v and in-quadrature output signal qv'. The transfer function of the input signal, v to the error signal ε_v is given by (4).

$$E(s) = \frac{\varepsilon_v}{v}(s) = \frac{s^2 + \omega'^2}{s^2 + k\omega' s + \omega'^2} \tag{4}$$

The Bode diagram shown in Fig. 3 is plotted for the transfer functions of E(s) and Q(s). It can be observed that the error signal and the in-quadrature output are in phase when the input frequency is lower than the SOGI resonant frequency ($\omega < \omega'$). The two signals are in counter phase when ($\omega > \omega'$). Therefore frequency error, ε_f can be defined as the product of qv' and ε_v. The average value of the frequency error will be positive when ($\omega < \omega'$), negative when ($\omega > \omega'$) and zero when ($\omega = \omega'$). The integral controller with a negative gain, $-\gamma$ can be used to make zero the dc component of the frequency error by shifting the SOGI resonance frequency ω' until the value is matching with the input frequency, ω. The input frequency will in this case be directly detected by the FLL.

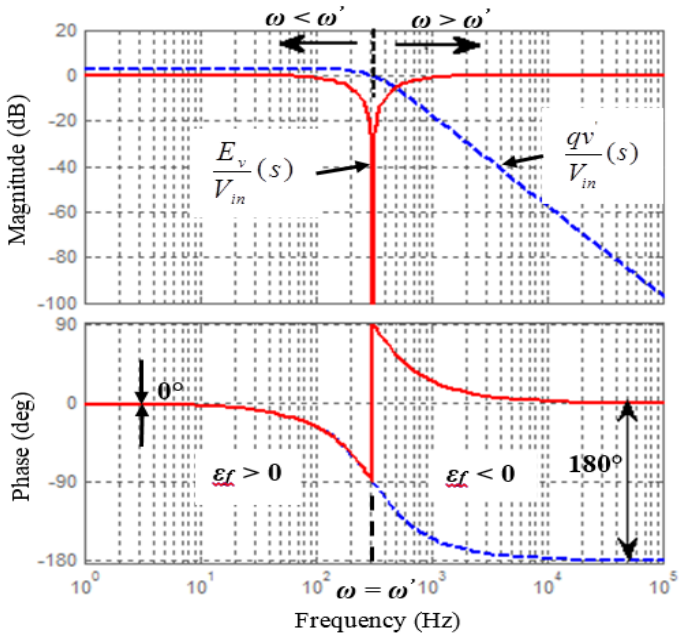

Fig. 3. Bode diagram of the input variables of FLL.

As shown in [38] the SOGI-QSG settling time can be calculated based on (5). In this case a settling time of 100ms in front of a frequency step has been considered.

Copyright (c) 2017 IEEE. Personal use is permitted. For any other purposes, permission must be obtained from the IEEE by emailing pubs-permissions@ieee.org.

This is the author's version of an article that has been published in this journal. Changes were made to this version by the publisher prior to publication.
The final version of record is available at http://dx.doi.org/10.1109/TIA.2017.2743200

$$t_{s(SOGI-QSG)} = \frac{10}{k\omega'} \tag{5}$$

By considering that the in-quadrature output of the SOGI-QSGs as the VF signal and that the direct output signal v' can be the considered as the derivative of the VF, two sets of 90° phase shifted signals needed for sequence separation will be available as part of the VF estimation. Thus, the per unit (p.u.) positive sequence VF components can be described in (6) and (7) respectively [29]-[31].

$$\chi_{\alpha}^{+}(s) = \frac{1}{2} qv'_{\alpha}(s) + \frac{1}{2} v'_{\beta}(s) \tag{6}$$

$$\chi_{\beta}^{+}(s) = \frac{1}{2} qv'_{\beta}(s) - \frac{1}{2} v'_{\alpha}(s) \tag{7}$$

2.3 Proportional Resonant Current Controller for the Inner Loop Control of VSC

In order to provide a smooth tracking capability and to achieve a zero error during the steady state condition, PR current controllers are applied for the inner current control loop of the inverter. The PR current controller can be described in ideal or non-ideal cases. The transfer function of the ideal PR current controller is shown in (8), and can be implemented by a SOGI.

$$G_{PR}(s) = K_p + K_r \frac{s}{s^2 + \omega_o^2} \tag{8}$$

However, in practical implementations, the non-ideal PR-controller is normally preferred because the ideal resonant term controller could cause stability problems due to its infinite gain. The transfer function of the PR current controller considering the non-ideal case is given in (9), where the term ω_c is the bandwidth around the ac frequency of ω_o [1].

$$G_{PR}(s) = K_p + K_r \frac{2\omega_c s}{s^2 + 2\omega_c s + \omega_o^2} \tag{9}$$

By widening or narrowing the ω_c, the bandwidth can be controlled. The smaller the value of ω_c, the more sensitive the filter is in front of frequency variations. In turn, K_p is the proportional gain and the K_r is the resonant gain of the system.

2.4 Current Reference Generation

The current reference generation for alpha and beta components in this work are relying on the equations stated in (10).

$$i_{\alpha}^{*} = \left[\frac{P_{ref} \cdot \chi_{g,\alpha}^{+} + Q_{ref} \cdot \chi_{g,\beta}^{+}}{\chi_{g,\alpha}^{+\,2} + \chi_{g,\beta}^{+\,2}} \right] + i_{cf,\alpha}, \qquad i_{\beta}^{*} = \left[\frac{P_{ref} \cdot \chi_{g,\beta}^{+} - Q_{ref} \cdot \chi_{g,\alpha}^{+}}{\chi_{g,\alpha}^{+\,2} + \chi_{g,\beta}^{+\,2}} \right] + i_{cf,\beta} \tag{10}$$

Copyright (c) 2017 IEEE. Personal use is permitted. For any other purposes, permission must be obtained from the IEEE by emailing pubs-permissions@ieee.org.

This is the author's version of an article that has been published in this journal. Changes were made to this version by the publisher prior to publication.
The final version of record is available at http://dx.doi.org/10.1109/TIA.2017.2743200

The positive sequence of the estimated VF is used for calculating a current reference that will provide balanced sinusoidal currents [16]. Furthermore, the estimated capacitor current i_{cf} is added to the current reference calculated from the VF estimated at the PCC, since the feedback signals for the current controllers is measured at the converter terminals. The reference signals for active and reactive power at the PCC are specified in (10) as P_{ref} and Q_{ref}. Thus, a good VF estimation at the PCC is essential for providing accurate control of the active and reactive power flow as well as for ensuring balanced sinusoidal current reference.

3. Implementation of VF Estimation with LCL Filter

3.1 Voltage Sensor-less VF Estimation; First method

Differently from classical grid synchronization approaches based on processing the grid voltage measurements, the concept of VF-based synchronization relies on estimation of the grid voltage conditions without any voltage sensor at the point where the active and reactive power flow should be controlled. By means of this method, the estimation depends on the measurement of the converter-side currents, i_{con}, which are later used to perform the subsequent transformations and estimations. The capacitor current, $i_{cf,\alpha\beta}$, will in this case be estimated based on the estimated VF at the filter capacitors. In order to avoid measuring additional currents, the grid current, $i_{g,\alpha\beta}$ is obtained by subtracting the estimated capacitor current from the converter current.

The estimated voltage drop across R_1 can be obtained by multiplying the converter current by R_1, and this voltage will be subtracted from the converter output voltage before estimating the VF. Thus, without considering the PNS separation, the VF at the filter capacitors could be estimated as (11),

$$\chi_c^{\alpha\beta}(t) = \underbrace{\left(m_{ref,\alpha\beta}\cdot v_{dc} - r_1\cdot i_{con,\alpha\beta}\right)\frac{k\omega'^2}{s^2+k\omega' s+\omega'^2}}_{\chi^{\int}_{\alpha\beta}} - l_1\cdot i_{con,\alpha\beta}(t) \tag{11}$$

where χ is the scaled virtual flux corresponding to the voltage integral multiplied by per unit frequency, ω_{pu} of the system.

The PNS components of the capacitor current can be attained based on the PNS components of VF estimated at the capacitor $\chi_c^{\alpha\beta+}$ and $\chi_c^{\alpha\beta-}$. The $\chi_c^{\alpha\beta+}$ and $\chi_c^{\alpha\beta-}$ can be calculated by subtracting the induced PNS components of flux in L_1 from the output of the DSOGI-VF. Consequently, this estimation also depends on the PNSC of the converter currents. Considering $\chi^{\int+}_{\alpha\beta}$ as the positive sequence flux component resulting from the DSOGI-VF estimation with inherent sequence separation, the positive sequence VF, $\chi_c{}^{\alpha\beta+}$ at the filter capacitor can be expressed by (12).

Copyright (c) 2017 IEEE. Personal use is permitted. For any other purposes, permission must be obtained from the IEEE by emailing pubs-permissions@ieee.org.

This is the author's version of an article that has been published in this journal. Changes were made to this version by the publisher prior to publication.
The final version of record is available at http://dx.doi.org/10.1109/TIA.2017.2743200

$$\chi_c^{\alpha\beta+} = \chi_{\alpha\beta}^{\int+} - l_1 \cdot i_{con}^{\alpha\beta+} \tag{12}$$

The estimation is continued with the compensation for the resistive voltage drop on the virtual flux at the grid side of the LCL filter. Thus, influence from the resistive drop across the R_2 must be subtracted from the VF estimation at the filter capacitor. This is obtained by multiplying the integral of the grid current, ϑ_g with R_2. Before reaching the final estimation at the grid side, the induced flux drop at the grid side must be also subtracted. The induced flux drop can be calculated by multiplying the sum of L_2 and L_T by the PNSC of grid currents. In this work, the L_T is considered as the transformer leakage inductance, with a value of 6% of the base impedance value. The resulting VF estimation in the stationary reference frame, is given by (13).

$$\chi_g^{\alpha\beta+} = \chi_{\alpha\beta}^{\int+} - r_2 \cdot \vartheta_g^{\alpha\beta+} - (l_2 + l_T) \cdot i_g^{\alpha\beta+} \tag{13}$$

Where

$$i_g^{\alpha\beta+} = i_{con}^{\alpha\beta+} - i_{cf}^{\alpha\beta+} \tag{14}$$

Fig. 4 shows an overview of the method to obtain the PNS VF components estimated at the PCC, which is applicable to all the three methods that will be described in this paper. The method for obtaining the positive sequence of the virtual flux estimation with the subtraction of voltage drop across the resistor R_2 and the induced flux drop across inductor L_1 and L_2 as well as the inductor at the transformer is shown in a schematic in Fig. 5. The sequence separation of the converter and the capacitor currents as well as the grid current integral are graphically represented in Fig. 6 (a), while the block diagram for obtaining the estimation of the positive and negative sequence capacitor current is shown in Fig. 6 (b) respectively.

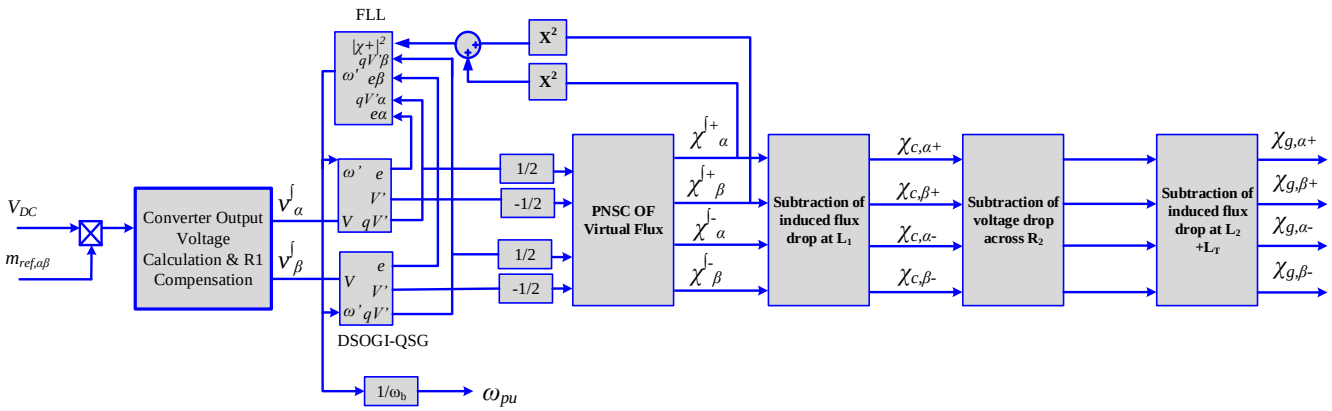

Fig. 4. Overview of VF estimation using voltage sensor-less method.

Copyright (c) 2017 IEEE. Personal use is permitted. For any other purposes, permission must be obtained from the IEEE by emailing pubs-permissions@ieee.org.

This is the author's version of an article that has been published in this journal. Changes were made to this version by the publisher prior to publication.
The final version of record is available at http://dx.doi.org/10.1109/TIA.2017.2743200

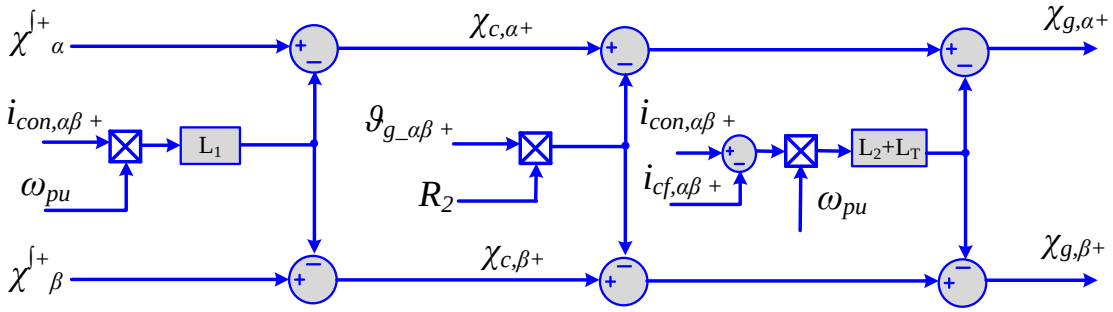

Fig. 5. Positive Sequence Virtual Flux Estimation.

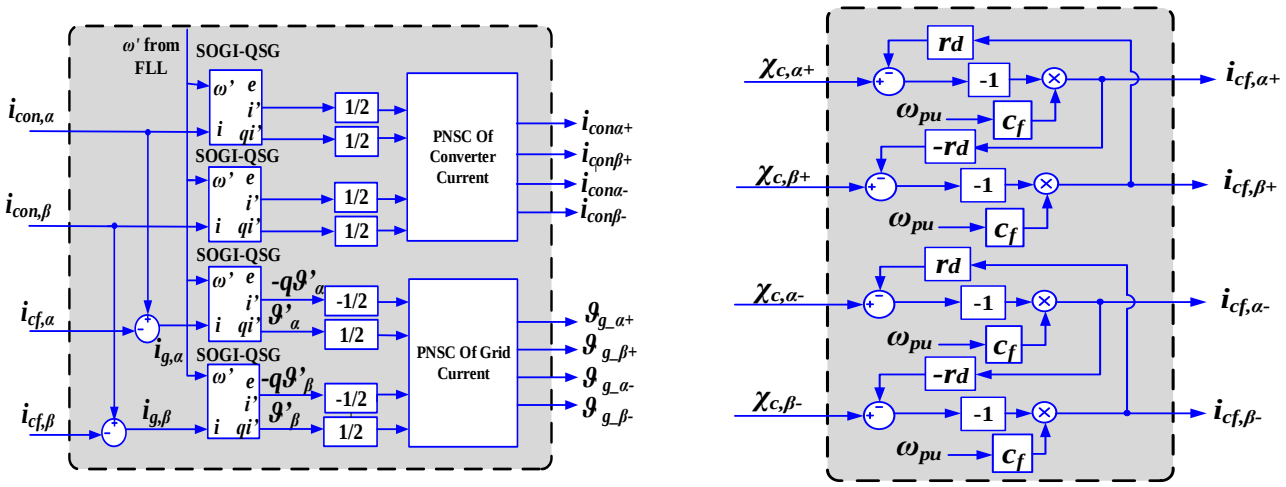

Fig. 6. Sequence Separation of current and grid current integral. (a) Grid Current integral and sequence separation of converter and grid current for Method 1 and Method 2, (b) Sequence separation of capacitor current for Method 1 and Method 2.

3.2 VF Estimation with voltage sensors at the filter capacitors; Second Method

In this second method, voltage sensors are used to measure the capacitor voltage, v_f. Considering that the capacitor voltage is now measured, the PNS components of the VF at the filter capacitors can be obtained directly as shown in Fig. 7 and used as input to the capacitor current estimation shown in Fig. 6 (b).

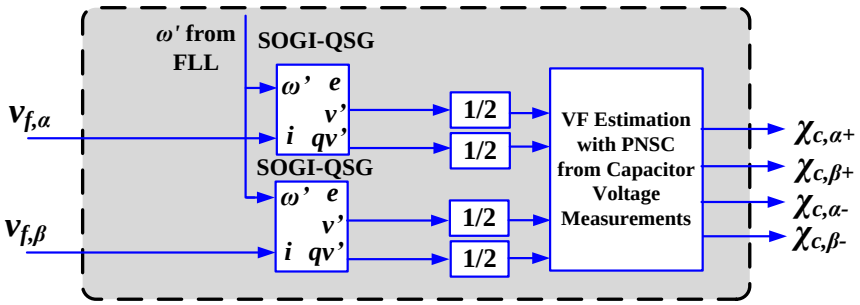

Fig. 7. PNS components of the VF at the filter capacitors

Copyright (c) 2017 IEEE. Personal use is permitted. For any other purposes, permission must be obtained from the IEEE by emailing pubs-permissions@ieee.org.

This is the author's version of an article that has been published in this journal. Changes were made to this version by the publisher prior to publication.
The final version of record is available at http://dx.doi.org/10.1109/TIA.2017.2743200

In a practical implementation, measuring the capacitor voltage is not always a significant extra cost, and voltage sensors will be commonly included in the LCL filter configuration from Fig. 1. Thus, voltage measurements could be used for the current estimation. The voltage measurements could also be used for directly estimating the PNS VF components at the filter capacitors, but in case of voltage sensor failure an approach with VF estimation from the converter voltage and current could be more reliable. Thus, in the following it will be assumed that voltage sensors are used only for the capacitor current estimation, and not for the VF estimation at the filter capacitors. Thus, the block diagram shown in Fig. 4 and Fig. 5 as well as the expression given by (11)-(14) are still valid for obtaining the resulting VF estimation in this case. However the PNS VF components obtained from the voltage measurements in Fig. 7 could be compared to the estimation from the converter currents, and any deviations could be utilized for correcting the parameters of the voltage-sensor-less VF estimation.

3.3 VF Estimation with additional current sensor to obtain capacitor current; Third method

In this method, the current sensor is used to measure the capacitor current, i_{cf} directly. Following the same implementation as in the previous two methods, the estimation of the converter output voltage as well as the positive and negative sequence component of the virtual flux estimation is based on the schemes from Fig. 4 and Fig. 5. The only difference in this case is that the block diagram of the capacitor current estimation is not necessary. This third method can be summarized by Fig. 8, where the capacitor current appears as a direct measurement. In this method, four sets of DSOGI-QSGs and PNS estimation blocks are considered, compared to only three sets required in method 1 and 2. Indeed, an additional set of DSOGI-QSGs with PNS estimation are required to obtain the positive and negative sequence of capacitor currents as shown in Fig. 8. The grid current integral ϑ_g is still necessary, since this current is also included in the VF estimation. Following the same approach used in the previous methods, the grid current is obtained by subtracting the capacitor current from the converter current before it is integrated to obtain the PNS. In this method, the expression described in (13) is still valid for obtaining the estimated VF at the PCC.

Copyright (c) 2017 IEEE. Personal use is permitted. For any other purposes, permission must be obtained from the IEEE by emailing pubs-permissions@ieee.org.

This is the author's version of an article that has been published in this journal. Changes were made to this version by the publisher prior to publication.
The final version of record is available at http://dx.doi.org/10.1109/TIA.2017.2743200

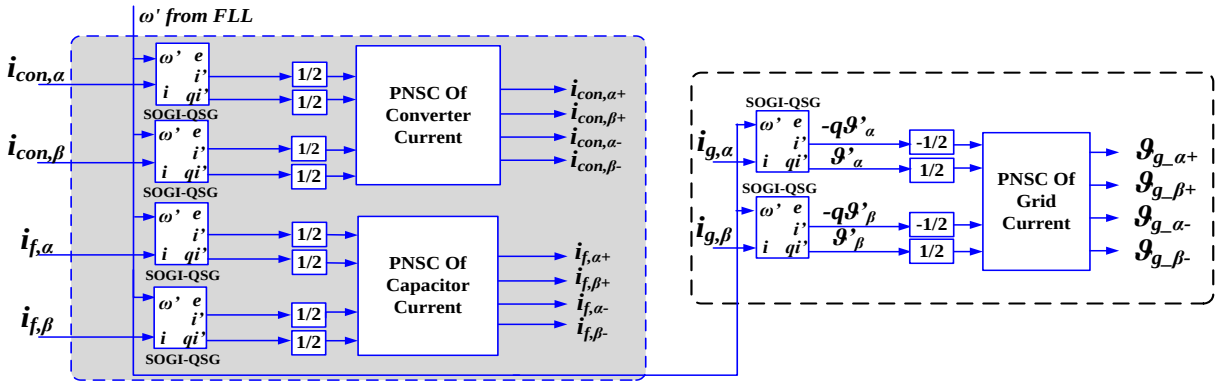

Fig. 8. Grid current integral and sequence separation of converter and capacitor current for Method 3.

4. Simulation Results of VF Estimation

Based on the structure of the investigated system shown in Fig. 1, an overview of the complete configuration for the simulation studies is shown in Fig. 9.

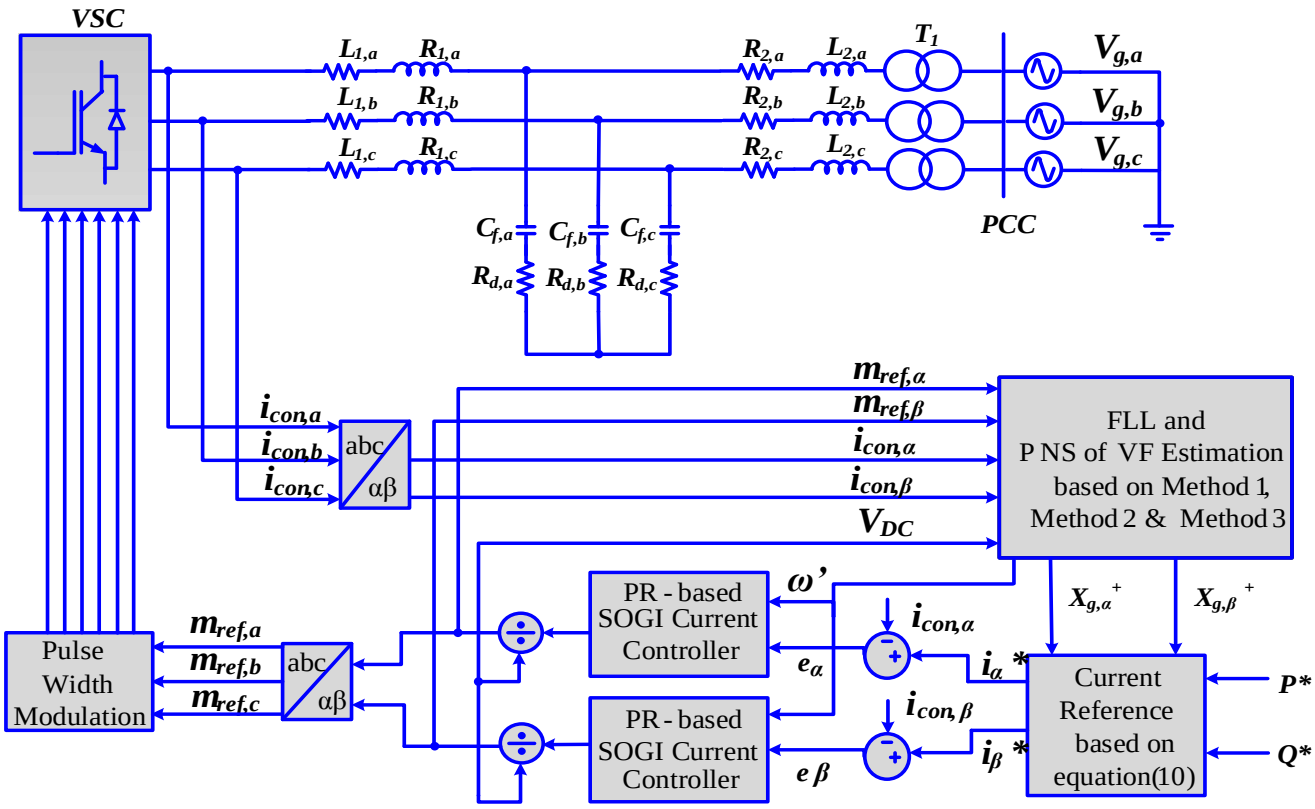

Fig. 9. Simulation Setup.

In this work, 10 kHz is selected as switching frequency and as sampling frequency for the control system of the 10 kVA converter. This switching frequency is suitable choice for this range of power, as it has a good trade-off between sizing of passive

Copyright (c) 2017 IEEE. Personal use is permitted. For any other purposes, permission must be obtained from the IEEE by emailing pubs-permissions@ieee.org.

This is the author's version of an article that has been published in this journal. Changes were made to this version by the publisher prior to publication.
The final version of record is available at http://dx.doi.org/10.1109/TIA.2017.2743200

components, resulting ripple and total losses. If the switching and sampling is higher the proposed solution would still work well. The increasing speed of microprocessors permits to fit the VF algorithm in the pipeline. In the case of this paper, even the code is not optimized, the code is executed in less than half of a cycle.

The simulation has been carried out for all the three methods that have been proposed in section 3, using the parameters listed in Table 1. The design parameters listed in Table 1 are based on a 10 kW real power converter setup that will be later used in the experimental validation. The simulation studies have been conducted for two different scenarios.

Table 1. Simulation Parameters

Abbreviation	Nomenclature	Values
S_N	Rated Apparent Power	10 kVA
$V_g(p\text{-}p)$	Phase to Phase Grid Voltage	400 V
$V_g(p)$	Phase Voltage	230 V
V_{DC}	dc-link Voltage	700 V
$L_{1(abc)}$	Inductor, L_1	3.4 mH
$L_{2(abc)}$	Inductor, L_2	588 µH
$L_{T(abc)}$	Inductor, L_T	35.28 µH
$C_{f(abc)}$	Filter Capacitor	4.7 µF
$R_{d(abc)}$	Damping Resistor	1.8 Ω
f_{sw}	Switching Frequency	10 kHz
f_s	Sampling Frequency	10 kHz

4.1 Active and Reactive Power Injection.

The transient and steady state response of the system are monitored using the three VF based control methods when the active power and reactive power reference is set to, P_{ref} = 9 kW (0.9 p.u.) and Q_{ref} = 3 kVar (0.3 p.u.). The value of K_p = 7 and K_r =19 are used in both simulation and experimental. A step in the references from zero is applied at t = 0.1 s. and the collected results are presented in the time domain in p.u. values.

Copyright (c) 2017 IEEE. Personal use is permitted. For any other purposes, permission must be obtained from the IEEE by emailing pubs-permissions@ieee.org.

This is the author's version of an article that has been published in this journal. Changes were made to this version by the publisher prior to publication.
The final version of record is available at http://dx.doi.org/10.1109/TIA.2017.2743200

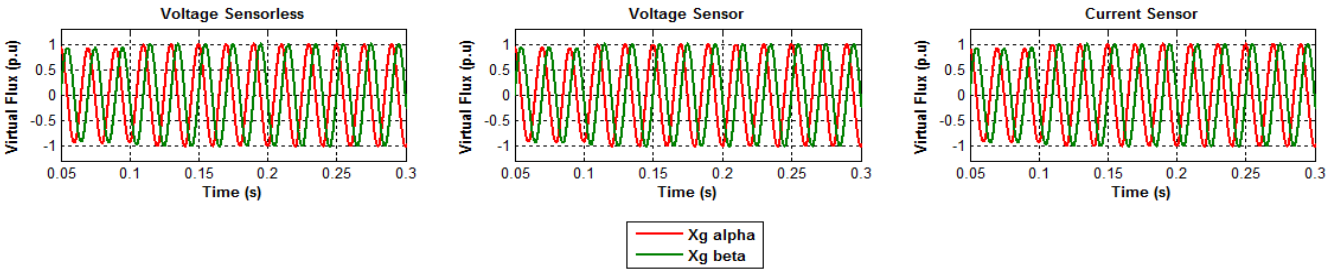

(a)

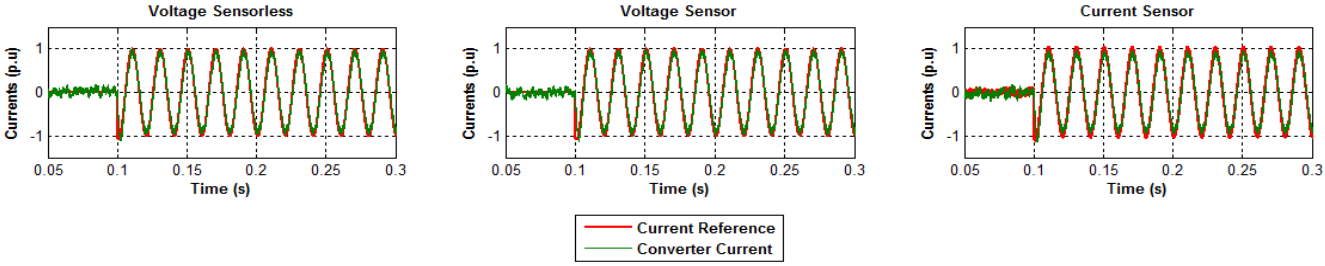

(b)

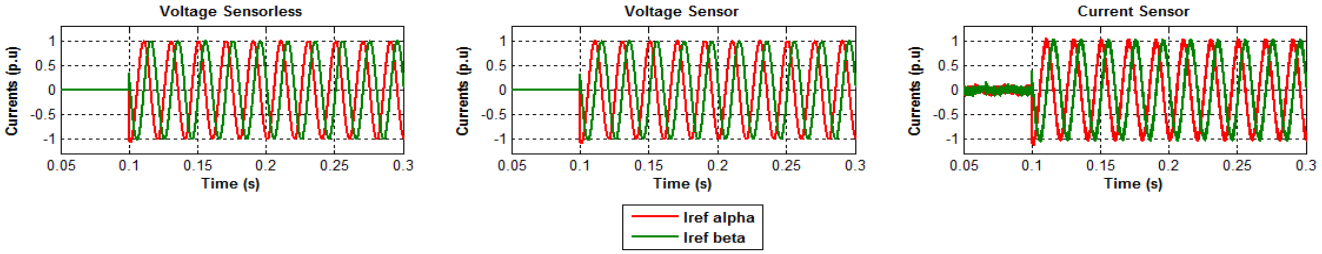

(c)

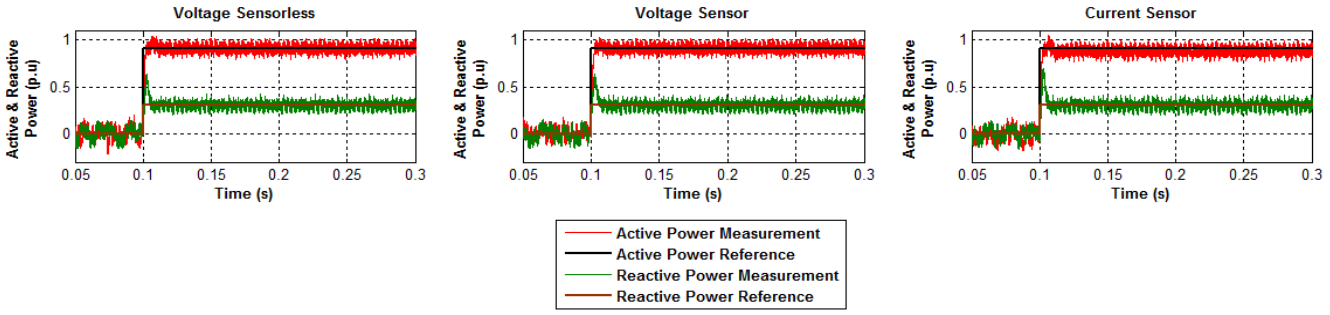

(d)

Copyright (c) 2017 IEEE. Personal use is permitted. For any other purposes, permission must be obtained from the IEEE by emailing pubs-permissions@ieee.org.

This is the author's version of an article that has been published in this journal. Changes were made to this version by the publisher prior to publication.
The final version of record is available at http://dx.doi.org/10.1109/TIA.2017.2743200

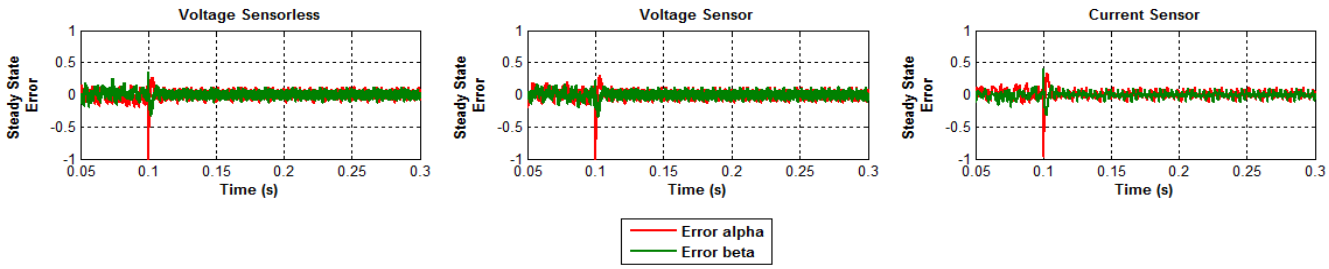

(e)

Fig. 10. Simulation Results. (a) Positive sequence of virtual flux estimation, (b) Tracking capability for all the three methods (c) Current reference generation at alpha and beta components (d) Active and reactive power measurement of the system (e) Steady state error.

As it can be seen from Fig. 10 the performance of the system with all the VF based methods is good. In Fig. 10 (a), it can be seen that the positive sequence of the virtual flux estimation in all methods is sinusoidal and balanced, as expected. In Fig. 10 (b), the tracking capability of the PR current controller is verified, as the system is able to follow the current reference generation almost immediately when the reference step has been applied, for all the three methods. The converter currents show no transients overshoot, however in the third method, where the capacitor current measurement is involved, there is a noticeable noise in the current as shown in Fig. 10 (c). This noise in the reference is due to the measured noise.

In Fig. 10 (d) the values of active power in the time domain match in all cases with the active power reference. Moreover, the proposed synchronization strategies are able to ensure that the active and reactive power injection to the grid is accurately controlled with only small overshoot in the measured reactive power occurring during the start-up for all the three cases. The overshoot is quickly compensated, and the system reach its steady state at approximately at t=0.103 s. The steady state error of the system is shown in Fig. 10 (e). These results confirm that the PR current controller used in the proposed system is able to eliminate the tracking error and achieve zero error during the steady state.

4.2 Change in Active and Reactive Power

Results from another simulation are presented in order to demonstrate that the system is working well when different values of active and reactive power are injected to the grid and the results of simulation is shown in Fig. 11. The values of P_{ref} and Q_{ref} that have been set in this simulation are the same values as in the previous simulation which are P_{ref} = 1 p.u. and Q_{ref} = 0.4 p.u. as well as P_{ref} = 0.7 p.u. and Q_{ref} = 0 p.u.

Copyright (c) 2017 IEEE. Personal use is permitted. For any other purposes, permission must be obtained from the IEEE by emailing pubs-permissions@ieee.org.

This is the author's version of an article that has been published in this journal. Changes were made to this version by the publisher prior to publication.
The final version of record is available at http://dx.doi.org/10.1109/TIA.2017.2743200

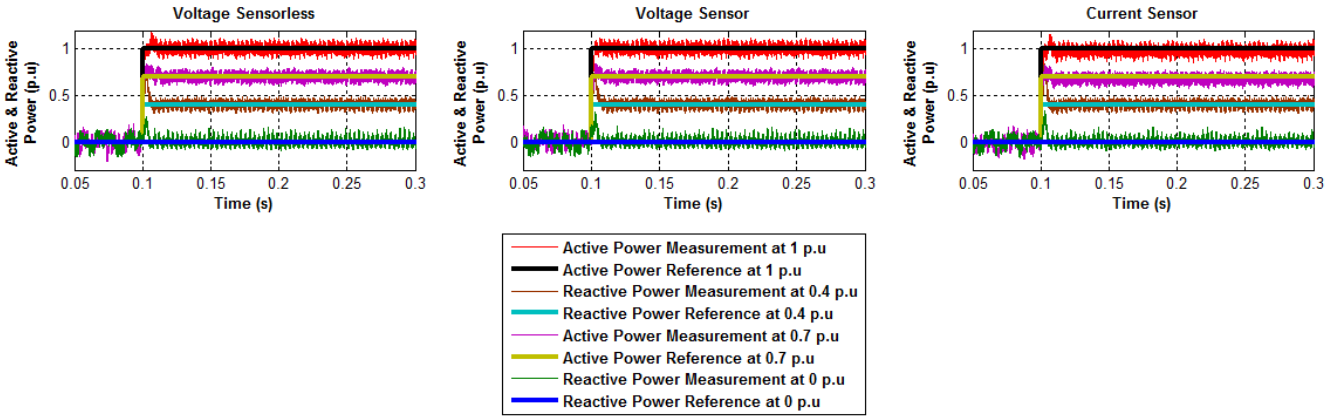

Fig. 11. Different injection of active and reactive power

As similar to the results shown in Fig. 10 (d), the system is working very well for different injections of active and reactive power and it can be seen that the active and the reactive power measurements match with the respective references. In general, the presented results rely on accurate VF estimation, since the synchronization with the grid and the corresponding control of the active and reactive power injection to the PCC is based on the VF signals. A good estimation and the capability of controlling the active and reactive power injections are desirable in order for the system to respond to the variation of voltage and frequency. By using the DSOGI-FLL in the virtual flux estimation, the system is inherently adaptive to frequency variations, and it is able to provide a very fast response.

5. Experimental Results of VF Estimation

The experimental setup used for the final validation consists of a 10 kVA inverter which is connected to a three phase ac power source through a LCL filter. The inverter is powered by a dc-power supply that provides a 700 V dc-link voltage. The controller of the whole system is embedded in a dSpace1103 platform, which controls the switches of the converter through fibre-optic links. An image of the experimental setup is shown in Fig. 12 (a), while a block diagram showing the system configuration is shown in Fig. 12 (b). The parameters of the system are the same as listed in Table 1 and the results have been structured into SCADA layout. The SCADA layout is built using the control desk application of dSpace.

Copyright (c) 2017 IEEE. Personal use is permitted. For any other purposes, permission must be obtained from the IEEE by emailing pubs-permissions@ieee.org.

This is the author's version of an article that has been published in this journal. Changes were made to this version by the publisher prior to publication.
The final version of record is available at http://dx.doi.org/10.1109/TIA.2017.2743200

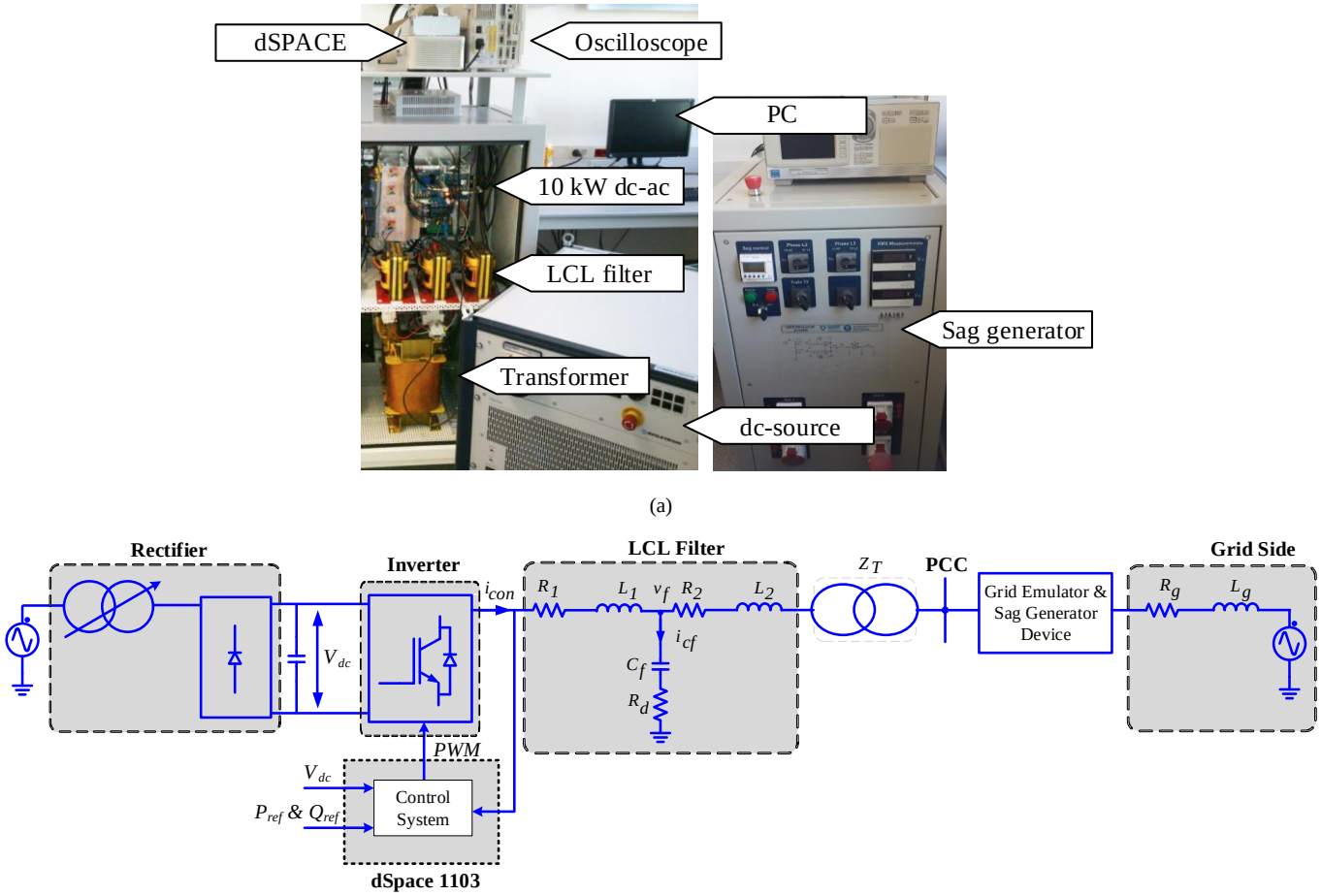

Fig. 12. (a) Experimental setup in the lab, (b) block diagram of the experimental setup.

In the experimental system the overcurrent protection includes also an anti-saturation block, which will ensure that the current will be always in the non-saturated range. Saturation of the phase current waveforms should be avoided in the experiment as it may cause a current distortion larger than the expected. In any case this limitation is also necessary in real power converter, as the THD should be lower than 3-4% in order to comply with harmonic emission standards.

Considering the VF estimation methods explained in section 3, the approach without additional ac-side voltage or current sensors requires a more complex structure for implementation than method 2 and 3. As this method is relying on the converter output current as the only ac-side measurement, it is also considered the most challenging one from the experimental implementation point of view. If this method works and provides similar results from the experimental platform as obtained from the simulations, it can be assumed that the performance of method 2 and method 3 can be assessed according to the simulation results. Thus, only results from experimental verification of method 1 will be presented.

Copyright (c) 2017 IEEE. Personal use is permitted. For any other purposes, permission must be obtained from the IEEE by emailing pubs-permissions@ieee.org.

This is the author's version of an article that has been published in this journal. Changes were made to this version by the publisher prior to publication.
The final version of record is available at http://dx.doi.org/10.1109/TIA.2017.2743200

5.1 Active and Reactive Power Control

The value of K_p and K_r used in the experimental setup are the same as ones used in the simulation. The plots in Fig. 13 show the experimental results where a power step of 0.9 p.u. of in the active power reference has been applied at t = 0.1 s. In this experiment, the reactive power reference has been set to 0 p.u.

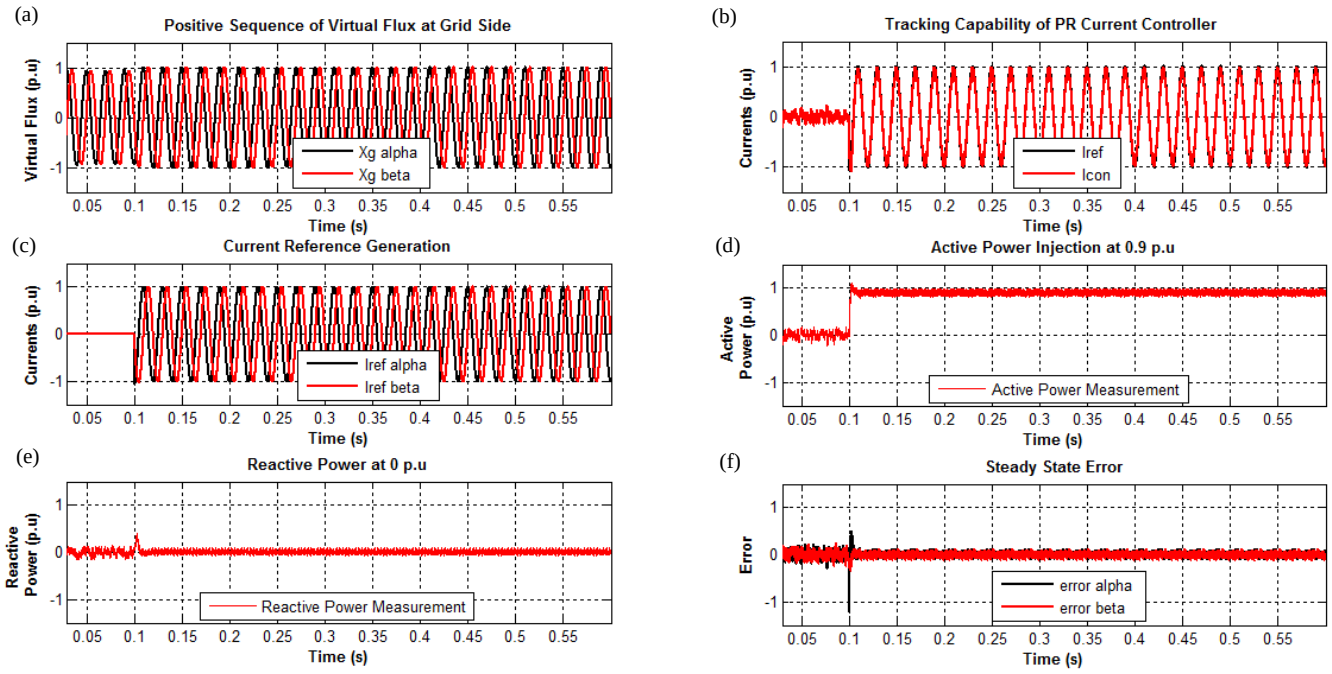

Fig. 13. Experimental results taken from the control desk.

The experimental results shown in Fig. 13 validate the simulation results shown in Fig. 10. The results also confirm that with a stable value of the filter parameters, the accuracy of the VF estimation is ensured, providing a good basis control of the active and the reactive power at the PCC. As in the simulations, the current feedback signal is measured at the converter side. Therefore, the estimated capacitor current must be included in the calculation of the current reference, according to (10). As it is proven in the plots, the proposed system tracks the reference with fast dynamic response and has zero steady state error. The positive sequence of the VF estimation shown in Fig. 13 (a) shows that the proposed control is able to estimate accurately the grid voltage conditions. The curves in Fig. 13 (a), also show how the estimation yields a clean, balanced, sinusoidal signal with a beta component lagging the alpha component by 90°. Both signals show that the virtual flux estimations at the grid side are free from the ripple and distortion.

A good result of VF estimation as well as a good tuning of K_p and K_r contributes to a good current tracking capability, avoiding any transient overshoot, as it can be concluded from Fig. 13 (b). In turn, the efficiency of VF estimation as well as accurate estimation of the capacitor current ensures balanced sinusoidal current references, as shown in Fig. 13 (c), which are

Copyright (c) 2017 IEEE. Personal use is permitted. For any other purposes, permission must be obtained from the IEEE by emailing pubs-permissions@ieee.org.

This is the author's version of an article that has been published in this journal. Changes were made to this version by the publisher prior to publication.
The final version of record is available at http://dx.doi.org/10.1109/TIA.2017.2743200

appropriately synchronized to the voltages in the system. Due to the proper VF estimation, the proposed system is able to control both active and reactive power without any errors as shown in Fig. 13 (d) and (e). The steady state error shown in Fig. 13 (f) prove that the PR-current controller is working as required, eliminating the steady state error.

5.2 Change in Active Power Injection

Another test with different values of active power injection was carried out in order to observe the performance of the proposed system. The results obtained in this case are shown in Fig. 14, where it can be seen that the reference step change has been set to 1 p.u. and 0.8 p.u. respectively. By observing the results shown in both Fig. 14 (a) and Fig. 14 (b), it can be concluded that the proposed system is able to control the active power perfectly without any noticeable overshoot in the transient response. Thus, the VF estimation and the power control at grid side are working properly.

The instantaneous power theory has been used to measure the active power, without including any filter. This is the reason why the power has a small ripple, due to the inherent noise in the acquisition system boosted also by the relatively high impedance of the experimental grid. However, the harmonic content in the current is below 2% (while up to 4% is admitted) and the performance of the overall controller is not affected. Moreover, this ripple could be considered as a proof that the system is able to work even if the sensing is not perfect or if the voltage is affected by some distortion.

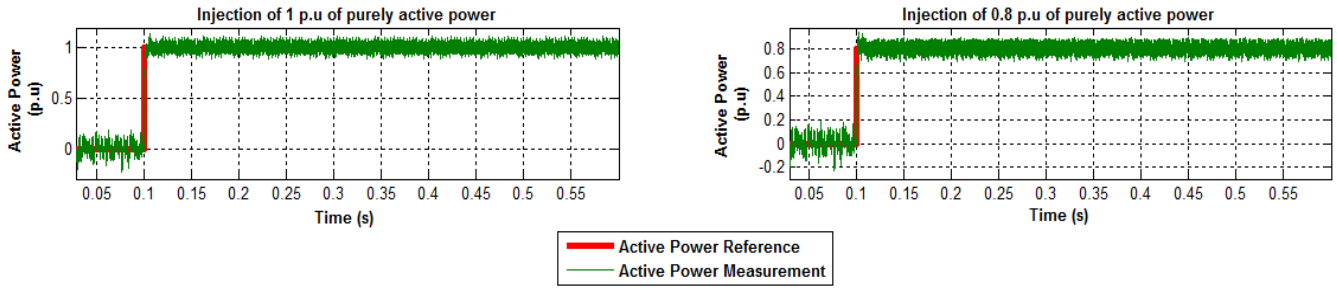

(a) (b)

Fig. 14. Purely active power injection

Copyright (c) 2017 IEEE. Personal use is permitted. For any other purposes, permission must be obtained from the IEEE by emailing pubs-permissions@ieee.org.

This is the author's version of an article that has been published in this journal. Changes were made to this version by the publisher prior to publication.
The final version of record is available at http://dx.doi.org/10.1109/TIA.2017.2743200

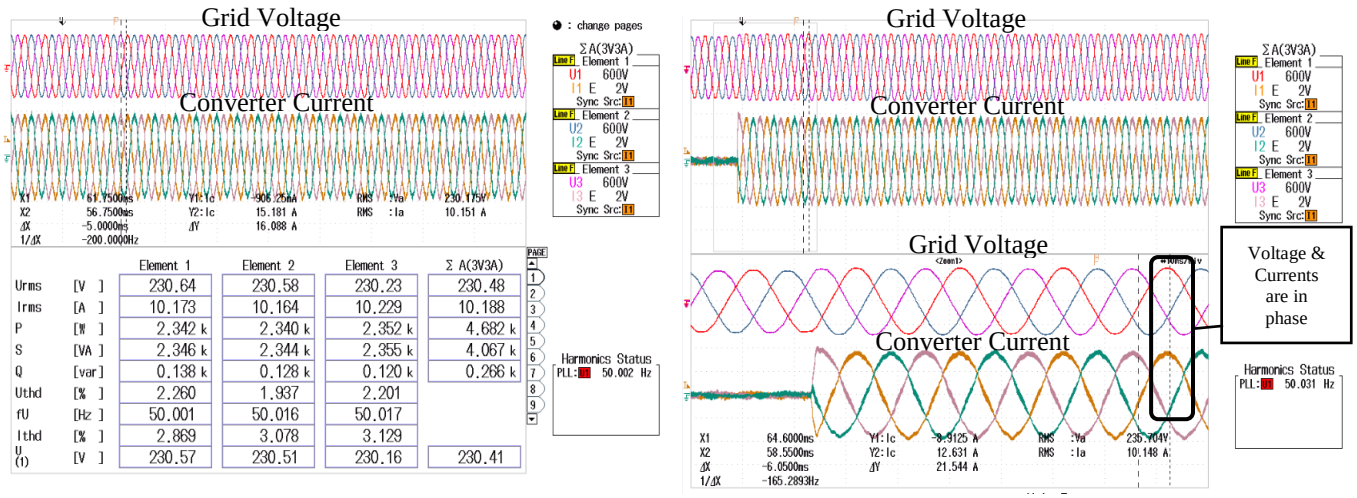

(a) (b)

Fig. 15. Converter currents and grid voltage captured from the oscilloscope when injecting purely active power.

Fig. 15 (a) shows the converter currents and grid voltage waveform for the case of 7.5 kW (0.75 p.u) power delivery. The waveform shown in Fig. 15 is used to compare the results obtained between the virtual flux estimation at the grid side that is available on the control desk with the grid voltage shown on the oscilloscope. When purely active power is injected, the peak of the grid voltages and the peak of the converter currents are in phase. This condition can be seen clearly in Fig. 15 (b) where the peak of the grid voltage, U1 and the peak of the converter current I1 are exactly in phase.

5.3 Change in Reactive Power Injection

Fig. 16 shows both active and reactive power injections considering two different steady state values for the active power and two different step changes in the reactive power reference. In Fig. 16 (a), the system injects 0.7 p.u. of active power, and experiences a reactive power step change of 0.4 p.u. Likewise, Fig. 16 (b) shows the performance of the system when the active power is 0.8 p.u. and step of 0.2 p.u. of reactive power is produced. Based on the results obtained in Fig. 16, it can be seen that the proposed system is able to control the active and the reactive power without any cross-coupled transients.

Copyright (c) 2017 IEEE. Personal use is permitted. For any other purposes, permission must be obtained from the IEEE by emailing pubs-permissions@ieee.org.

This is the author's version of an article that has been published in this journal. Changes were made to this version by the publisher prior to publication.
The final version of record is available at http://dx.doi.org/10.1109/TIA.2017.2743200

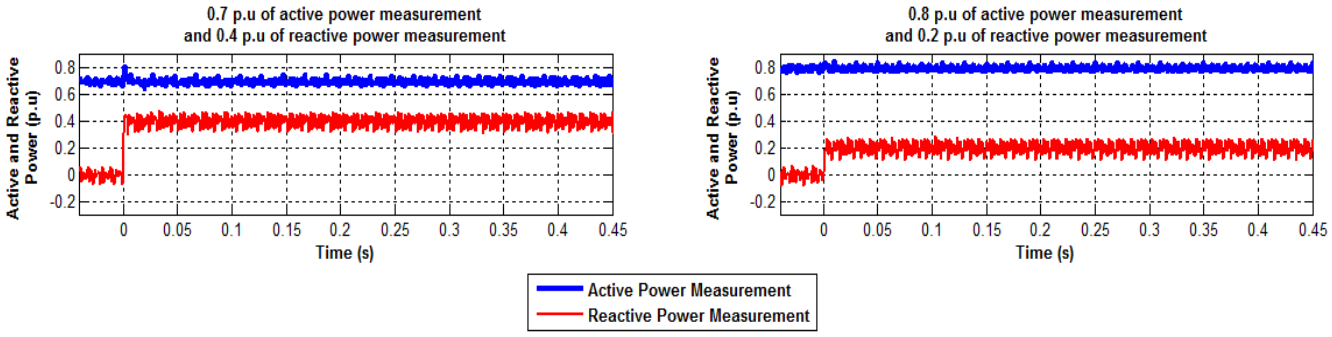

(a) (b)

Fig. 16. Active and reactive power injection to the grid.

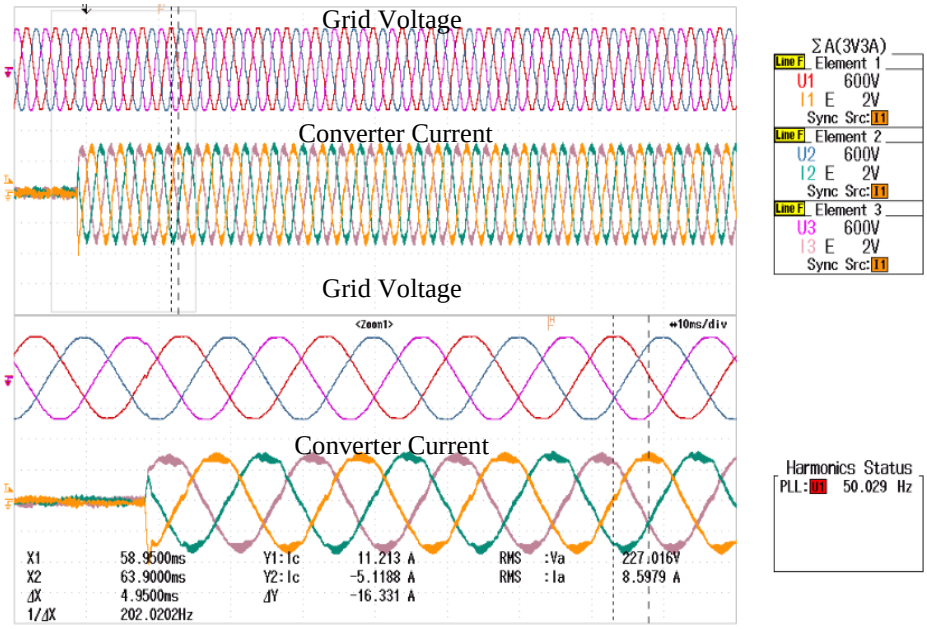

Fig. 17. Purely reactive power injection.

Fig. 17 shows the waveform of converter currents and grid voltage when 6 kVar (0.6 p.u) purely reactive power is injected to the system. When purely reactive power is injected, it can be seen that the converter current, I1 lags the grid voltage, U1 by approximately 90°. Considering that the system is working at 50Hz fundamental frequency, the time for one full cycle is equal to 20ms. Since one full cycle is equivalent to 360°, the phase displacement ΔX = 4.95ms indicated in the figure correspond to a 89.1° phase lag [(360° x 4.95ms)/20ms]. By observing the results shown in Fig. 14 to Fig. 17, it can be concluded that the first method discussed in section III has a good experimental performance, which accurately corresponds to the results from the simulations. Since this is the most complex method, among the three considered synchronization strategies, as it depends only on estimated values, it can be assumed that the performance of the other two methods can be assessed on basis of the simulation results.

Copyright (c) 2017 IEEE. Personal use is permitted. For any other purposes, permission must be obtained from the IEEE by emailing pubs-permissions@ieee.org.

This is the author's version of an article that has been published in this journal. Changes were made to this version by the publisher prior to publication.
The final version of record is available at http://dx.doi.org/10.1109/TIA.2017.2743200

Even though the grid voltage is not a global magnitude, it should be remain stable within certain limits over the electrical network. In order to ensure this condition, a precise control of active and reactive power is essential and the proposed system presented in this paper is able to provide an accurate power injection to the grid. Thus, the minor power ripple variations appearing in the results should not affect the stability of the system.

6. Conclusions

This paper has presented a comparative study of three different implementations of VF estimation for grid synchronization of a VSC with LCL filter, which permit to control the active and reactive power flow at the grid side of the filter. The results from simulation of all the three methods confirm that accurate parameters of the connection filter, as well as a good current measurement, are crucial to ensure a good estimation of the grid voltage conditions, which is necessary for controlling the active and reactive power injected to the grid at the PCC. The fast synchronization and the smooth reference tracking achieved in transient conditions, have demonstrated the effectiveness of the DSOGI-VF and the PR current controller used in the proposed system.

Among the investigated methods, the VF estimation based on voltage sensor-less operation offers several advantages in terms of cost reduction and improvement of the system modularity. However, for most practical applications, the measurement of the capacitor voltages is not a significant disadvantage. This voltage measurement can provide a stable output which can contribute positively to carry out an accurate estimation of the virtual flux at the PCC. However, when combined with VF-estimation, the synchronization method can also maintain operation in case of voltage sensor failure. On the other hand, placing a current sensor for measuring directly the capacitor current has been shown to be a less preferable solution, since the ripple current in the capacitor is very large compared to the fundamental frequency component. Thus, noise and ripple components might propagate into the control system and deteriorate the performance of the VF estimation.

The experimental verification has demonstrated that the VF approach based entirely on estimated signals for the LCL filter configuration can provide a good grid synchronization for control of the power delivered to the PCC. Among the three investigated estimation methods, this voltage sensor-less scheme was selected for validation, as it is the most complex scenario, and the achieved results permit also to validate the performance of the other two methods presented.

Acknowledgment

This work has been partially supported by the Ministry of Economy and Competitiveness under the projects ENE2014-60228 and ENE2016-79493-R. Any opinions, findings and conclusions or recommendations expressed in this material are those of the authors and do not necessarily reflect those of the host institutions and funders.

Copyright (c) 2017 IEEE. Personal use is permitted. For any other purposes, permission must be obtained from the IEEE by emailing pubs-permissions@ieee.org.

This is the author's version of an article that has been published in this journal. Changes were made to this version by the publisher prior to publication.
The final version of record is available at http://dx.doi.org/10.1109/TIA.2017.2743200

References

[1] R. Teodorescu, M. Liserre and P. Rodriguez, "Grid Converters for Photovoltaic and Wind Power Systems," John Wiley & Son, United Kingdom, 2011, pp. 1–4.

[2] A. Teke and M. B. Latran, "Review of multifunctional inverter topologies and control schemes used in distributed generation systems", *Journal of Power Electronics*, vol. 14, no. 2, pp. 324–340, Mar. 2014.

[3] J. Zhang, H. Wang, M. Zhu and X. Cai, "Control Implementation of the Full-Scale Wind Power Converter without Grid Voltage Sensors," in *Proc. 2014 International Power Electronics Conference*, Hiroshima, Japan, 2014, pp. 1753-1760.

[4] M. Davari, and Y. Mohamed, "Robust DC-Link Voltage Control of a Voltage-Source Converter Interfacing a Wind Turbine into DC-Grids", *IEEE Transactions on Power Electronics*, vol. 8993, no. c, pp. 1–1, Jan. 2016.

[5] C. Li, P. Zhan, J. Wen, M. Yao, N. Li, and W. J. Lee, "Offshore wind farm integration and frequency support control utilizing hybrid multiterminal HVDC transmission", *IEEE Transactions on Industry Applications*, vol. 50, no. 4, pp. 2788–2797, Jul/Aug 2014.

[6] P. Mitra, L. Zhang, and L. Harnefors, "Offshore wind integration to a weak grid by VSC-HVDC links using power-synchronization control: A case study", *IEEE Transactions on Power Delivery*, vol. 29, no. 1, pp. 453–461, Feb. 2014.

[7] D. Jovcic, L. Zhang, and M. Hajian, "LCL VSC converter for high-power applications", *IEEE Transactions on Power Delivery*, vol. 28, no. 1, pp. 137–144, Jan. 2013.

[8] K. J. Lee, J. P. Lee, D. Shin, D. W. Yoo, and H. J. Kim, "A novel grid synchronization PLL method based on adaptive low-pass notch filter for grid-connected PCS", *IEEE Transactions on Industrial Electronics*, vol. 61, no. 1, pp. 292–301, Jan. 2014.

[9] M. Boyra and J. L. Thomas, "A review on synchronization methods for gridconnected three-phase VSC under unbalanced and distorted conditions," in *Proc. 14th European Conference on Power Electronics and Applications* (EPE 2011), Birmingham, United Kingdom, 2011, pp. 1-10.

[10] Z. Xin, X. Wang, and Z. Qin, "An Improved Second-Order Generalized Integrator Based Quadrature Signal Generator", *IEEE Transaction on Power Electronics*, vol. 31, no. 12, pp. 8068–8073, Dec. 2016.

[11] A. Luna, J. Rocabert, J. I. Candela, J. R. Hermoso, R. Teodorescu, F. Blaabjerg and P. Rodriquez, "Grid Voltage Synchronization for Distributed Generation Systems under Grid Fault Conditions", *IEEE Transactions on Industry Applications*, vol 51, no. 4, pp. 1–1, Jul/Aug 2015.

[12] L. Hadjidemetriou, E. Kyriakides, Y. Yang, and F. Blaabjerg, "A Synchronization Method for Single-Phase Grid Tied Inverters", *IEEE Transaction on Power Electronics*, vol. 31, no. 3, pp. 2139–2149, Mar. 2016.

[13] H. Gholami-Khesht, S. Golestan, and M. Monfared, "Low computational burden grid voltage estimation for grid connected voltage source converter-based power applications", *IET Power Electronics*, vol. 8, no. 5, pp. 656–664, 2015.

[14] Y. K. Tao, Q. H. Wu, W.H. Tang, and L. Wang, "Voltage sensorless predictive direct power control of three-phase PWM converters", *IET Power Electronics*, vol. 9, no. 5, pp. 1009–1018, 2016.

Copyright (c) 2017 IEEE. Personal use is permitted. For any other purposes, permission must be obtained from the IEEE by emailing pubs-permissions@ieee.org.

This is the author's version of an article that has been published in this journal. Changes were made to this version by the publisher prior to publication.
The final version of record is available at http://dx.doi.org/10.1109/TIA.2017.2743200

[15] Y. K. Tao, Q. H. Wu, W. H. Tang, and L. Wang, "Voltage sensorless predictive direct power control for renewable energy integration under grid fault conditions", in *Proc. 2015 IEEE Innovative Smart Grid Technologies - ISGT ASIA 2015*, Bangkok, Thailand, 2015, pp. 1-5.

[16] J. A. Suul, A. Luna, P. Rodríguez, and T. Undeland, "Virtual-flux-based voltage-sensor-less power control for unbalanced grid conditions", *IEEE Transactions on Power Electronics*, vol. 27, no. 9, pp. 4071–4087, Sep. 2012.

[17] M. Hu, L. Wu, and J. Hui, "Improved virtual flux oriented model predictive power control of grid inverters," in *Proc. 2015 IEEE 10th Conference on Industrial Electronics and Application,* Auckland, New Zealand, 2015, pp. 1111–1115.

[18] J. A. Suul and T. Undeland, "Impact of Virtual Flux Reference Frame Orientation on Voltage Source Inverters in Weak Grids," in *Proc. 2010 International Power Electronics Conference*, Sapporo, Japan, 2010, pp. 368-375.

[19] J. A. Suul, M. Molinas and P. Rodríguez, "Exploring the Range of Impedance Conditioning by Virtual Inductance for Grid Connected Voltage Source Converters," in *Proc. 2012 3rd IEEE PES International Conference and Exhibition on Innovative Smart Grid Technologies*, Berlin, Germany, 2012, pp. 1-9.

[20] A. Razali, A. Rahman, G. George, and N. Rahim, "Analysis and Design of New Switching Look-Up Table for Virtual Flux Direct Power Control of Grid Connected Three Phase PWM AC-DC Converter," *IEEE Transactions on Industry Applications*, vol. 51, no. 2, pp. 1189 – 1200, Mar/Apr. 2015.

[21] J. G. Norniella, J. M. Cano, G. A. Orcajo, C. H. Rojas, J. F. Pedrayes, M. F. Cabanas, and M. G. Melero, "Improving the dynamics of virtual-flux-based control of three-phase active rectifiers," *IEEE Transactions on Industrial Electronics*, vol. 61, no. 1, pp. 177–187, Jan. 2014.

[22] Hamid Eskandari-Torbati, Davood A Khaburi and Vahid Eskandari-Torbati, "Dead beat control of three phase PWM rectifier using virtual flux based Direct Power Control (DPC) and with no line voltage measurements," in *Proc. 6th Power Electronics, Drives Systems & Technologies Conference (PEDSTC)*, Tehran, Iran, 2015, pp. 375 – 382.

[23] A. M. Razali, M. A. Rahman, and N. A. Rahim, "Real-Time Implementation of d-q Control for Grid Connected Three Phase Voltage Source Converter," in *Proc. IECON 2014 – 40th Annual Conference of the IEEE Industrial Electronics Society,* Dallas, TX, USA, 2014, pp. 1733–1739.

[24] M. Malinowski, M. P. Kazmierkowski, S. Hansen, F. Blaabjerg, and G. D. Marques, "Virtual-flux-based direct power control of three-phase PWM rectifiers," *IEEE Transactions on Industry Applications,* vol. 37, no. 4, pp. 1019–1027, Jul/Aug. 2001.

[25] M. Malinowski, M. P. Kazmierkowski, and A. M. Trzynadlowski, "A comparative study of control techniques for PWM rectifiers in AC adjustable speed drives," *IEEE Transactions on Power Electronics*, vol. 18, no. 6, pp. 1390–1396, Nov. 2003.

[26] M. Malinowski, M. P. Kazmierkowski, and A. M. Trzynadlowski, "Review and comparative study of control techniques for three-phase PWM rectifiers", *Mathematics and Computers in Simulation*, vol. 63, no. 3, pp. 349–361, 2003.

Copyright (c) 2017 IEEE. Personal use is permitted. For any other purposes, permission must be obtained from the IEEE by emailing pubs-permissions@ieee.org.

This is the author's version of an article that has been published in this journal. Changes were made to this version by the publisher prior to publication.
The final version of record is available at http://dx.doi.org/10.1109/TIA.2017.2743200

[27] P. Antoniewicz, and M. P. Kazmierkowski, "Virtual-flux-based predictive direct power control of AC/DC converters with online inductance estimation", *IEEE Transactions on Industrial Electronics*, vol. 55, no. 12, pp. 4381–4390, Dec. 2008.

[28] A. Kulka, "Sensorless digital control of grid connected three phase converters for renewable sources," PhD Dissertation, Norwegian Univ. Sci. Technology, Trondheim, Norway, 2009.

[29] J. A. Suul,"Control of Grid Integrated Voltage Source Converters Under Unbalanced Conditions – Development of an Online Frequency Adaptive Virtual Flux Based Approach," PhD Dissertation, Norwegian University of Science and Technology, Trondheim, Norway, 2012.

[30] J. A. Suul, A. Luna, P. Rodriguez, and T. Undeland, "Frequency-adaptive Virtual Flux estimation for grid synchronization under unbalanced conditions," in *Proc. IECON 2010 - 36th Annual Conference on IEEE Industrial Electronics Society*, Glendale, AZ, USA, 2010, pp. 486–492.

[31] J. A. Suul, A. Luna, P. Rodríguez, and T. Undeland, "Voltage-Sensor-Less Synchronization to Unbalanced Grids by Frequency-Adaptive Virtual Flux Estimation," *IEEE Transactions on Industrial Electronics*, vol. 59, no. 7, pp. 2910–2923, Jul. 2012.

[32] G. Wrona, and K. Malon, "Sensorless Operation of an Active Front End Converter with LCL filter," in *Proc. 2014 IEEE 23rd International Symposium on Industrial Electronics, ISIE 2014*, Istanbul, Turkey, 2014, pp. 2697-2702.

[33] W. Gullvik, "*Modeling, Analysis and Control of Active Front End (AFE) Converter*," PhD Dissertation, Norwegian University of Science and Technology, Trondheim, Norway, 2007.

[34] W. Gullvik, L. Norum, and R. Nilsen, "Active Damping of Resonance Oscillations in LCL-Filters Based on Virtual Flux and Virtual Resistor," in *Proc. 12th European Conference on Power Electronics and Applications*, Aalborg, Denmark, 2007, pp. 1-10.

[35] R. Pöllänen, A. Tarkiainen, M. Niemelä, and J. Pyrhönen, "Supply Voltage Sensorless Reactive Power Control of DTC Modulation Based Line Converter with L- and LCL-Filters," in *Proc. 10th European Conference on Power Electronics and Applications (EPE 2003)*, Toulouse, France, 2003.

[36] N. F. Roslan, J. A. Suul, A. Luna, I. Candela, and P. Rodriguez, "A Simulation Study of Proportional Resonant Controller Based on the Implementation of Frequency- Adaptive Virtual Flux Estimation with the LCL Filter", in *Proc. 41st Annual Conference of IEEE Industrial Electronics Society (IECON 2015)*, Yokohama, Japan, 2015, pp 1934–1941.

[37] N. F. Roslan, J. A. Suul, A. Luna, J. Rocabert, I. Candela, and P. Rodriguez, "A Comparative Study of Methods for Estimating Virtual Flux at the Point of Common Coupling in Grid Connected Voltage Source Converters With LCL Filter", in *Proc. 2016 IEEE Energy Conversion Congress and Exposition (ECCE 2016)*, Milwaukee, WI, USA, 2016, pp. 0–5.

[38] P. Rodríguez, A. Luna, R. S. Muñoz-Aguilar, I. Etxeberria-Otadui, R. Teodorescu and F. Blaabjerg, "A Stationary Reference Frame Grid Synchronization System for Three-Phase Grid-Connected Power Converters Under Adverse Grid Conditions," *IEEE Transactions on Power Electronics*, vol 27, no. 1, pp. 99-112, Jan. 2012.

Copyright (c) 2017 IEEE. Personal use is permitted. For any other purposes, permission must be obtained from the IEEE by emailing pubs-permissions@ieee.org.